Establishing the relationship between the growth stage of a pituitary tumor and visual functions using the area of the zone of chiasmal pressure from the tumor

Iegorova E. S., Guk M. O., Ukrainets O. V.

SI «Romodanov Neurosurgery Institute, National Academy of Medical Sciences of Ukraine», Kyiv (Ukraine)

Встановлення залежності між стадією росту пухлини гіпофіза та зоровими функціями за допомогою площі зони тиску пухлини на хіазму

Єгорова К. С., лікар-офтальмолог, канд. мед. наук; **Гук М. О.,** лікар-нейрохірург, д-р мед. наук, професор; **Українець О. В.,** лікар-нейрохірург, доктор філософії

ДУ «Інститут нейрохірургії ім. акад. А. П. Ромоданова НАМН України», Київ (Україна)

Abstract

Purpose: *To develop a mathematical model of chiasmal compression using a computer model of the area of surface pressure from the tumor.*

Material and Methods: *We reviewed the medical records of 361 patients treated for compressive optic neuropathy due to pituitary adenoma (PA) at SI "Romodanov Neurosurgery Institute, NAMS of Ukraine" in 2018-2024. Patients underwent clinical neurological and ophthalmological examinations, magnetic resonance imaging (MRI), computed tomography (CT) and functional studies. Mathematical modeling was done in cooperation with the Department of Software Engineering in Energy Industry, National Technical University of Ukraine "Igor Sikorsky Kyiv Polytechnic Institute". The study was based on modeling and statistical analysis.*

Results: *Patients (54.7% were women and 45.3% were men; mean age, 54.3 ± 12.5 years) were divided into 3 groups: group 1, early stage (small PAs, n = 115), group 2, moderately advanced stage (moderate-size PAs, n = 157), and group 3, advanced stage (giant PAs, n = 89). The difference between groups was statistically significant ($p < 0.05$). The study has confirmed the efficacy of using both CT and MRI for assessing tumor size. A mathematical model ($z = 377.38 + 122.19x – 2.25y – 77.74x^2 – 2.91xy + 0,02y^2$) was developed for predicting the area of pressure zone from a PA. Critical thresholds of the area of the zone of chiasmal pressure from a PA were determined. An especially abrupt decline in retinal nerve fiber layer (RNFL) thickness was noted as pressure zone area (PZA) exceeded 200 conventional units (CU), and the worst visual acuity (VA; 0.42) and RNFL thickness (40 μm) values were noted for a PZA of 300 CU.*

Conclusion: *The model proposed has some substantial advantages compared to those developed previously. It is based on a complex approach that combines clinical data from various diagnostic modalities with mathematical modeling. This allows taking in account multiple parameters such as PZA, VA and RNFL thickness. High model fitness ($R^2 = 0.9910$) and clear correlations between parameters provide for a reliable prediction of the PZA. This has an important practical value for detecting the pathology and planning the treatment strategy early.*

Keywords: *mathematical modeling, 3D modeling, pituitary adenoma, compressive optic neuropathy, optic chiasm, surface pressure area.*

Резюме

Мета: *Побудова математичної моделі хіазмальної компресії із застосуванням комп'ютерної моделі площі поверхневого тиску пухлини.*

Матеріал та методи. *Дослідження побудовано на результатах аналізу 361 пацієнта з компресійною оптичною нейропатією внаслідок аденоми гіпофіза (АГ), які знаходилися під спостереженням та отримували лікування на базі відділення ендоназальної нейрохірургії осно-*

DOI: https://doi.org/10.31288/Ukr.j.ophthalmol.202616370

UDC: 617.7

Corresponding Author: Yegorova Katerina Sergeevna. Candidate of Medical Sciences, Senior Research Fellow, Ophthalmologist, Neuro-Ophthalmology Department, The State Institution Romodanov Neurosurgery Institute National Academy of Medical Sciences of Ukraine. Address: 32 P. Maiboroda St., Kyiv, 04050, Ukraine. Email: iegorova_katya@ukr.net

Received 2025-02-19

Accepted 2026-01-16

Cite this article as: Iegorova KS, Guk MO, Ukrainets OV. Establishing the relationship between the growth stage of a pituitary tumor and visual functions using the area of the zone of chiasmal pressure from the tumor. Ukrainian Journal of Ophthalmology. 2026;(1):63-70.

ви черепа та групи нейроофтальмології ДУ «Інститут нейрохірургії ім. акад. А. П. Ромоданова НАМН України», в період 2018–2024 рр. Всім хворим проводилося клініко-неврологічне, офтальмологічне обстеження, використовувались інструментальні методи діагностики. Виконувався комплекс нейровізуалізуючих обстежень: магніторезонансна томографія (МРТ), комп'ютерна томографія (КТ).

Математичне моделювання проведено спільно з кафедрою інженерії та програмного забезпечення в енергетиці Національного технічного університету України «Київський політехнічний інститут імені Ігоря Сікорського». Дослідження базуються на моделюванні та статистичному аналізі, що відображає типову картину для подібних досліджень.

Результати. *У дослідженні взяв участь 361 пацієнт, усі вони були розділені на групи: I група – рання стадія (невеликі АГ, n=115), II група – помірна стадія (середні АГ, n=157), III група – важка стадія (велетенські та гігантські АГ, n= 89). Гендерний розподіл склав 54,7% жінок та 45,3% чоловіків, із середнім віком 54,3 ± 12,5 року. Різниця між групами виявилася статистично значущою (p <0,05).*

Дослідження підтвердило ефективність комплексного застосування КТ та МРТ для оцінки розмірів пухлини. Розроблена математична модель для прогнозування ($z = 377{,}38 + 122{,}19x – 2{,}25y – 77{,}74x^2 – 2{,}91xy + 0{,}02y^2$) дозволяє передбачати площу зони тиску. Визначено критичні пороги тиску на хіазму, де значення 200 умовних одиниць є переломним, а при досягненні 300 умовних одиниць спостерігаються найгірші показники з гостротою зору 0,42 та товщиною волокон 40 мкм.

Висновки. *Запропонована модель має ряд суттєвих переваг порівняно з попередніми дослідженнями. По-перше, вона базується на комплексному підході, що поєднує клінічні дані з математичним моделюванням. Це дозволяє врахувати множинні параметри, такі як площа тиску, гострота зору та товщина нервових волокон. Висока точність моделі ($R^2 = 0{,}9910$) та чіткі кореляційні зв'язки між параметрами забезпечують надійність прогнозування. Це має важливе практичне значення для раннього виявлення патології та планування лікувальної тактики.*

Ключові слова: *математичне моделювання, 3D моделювання, аденома гіпофіза, компресійна оптична нейропатія, хіазма, площа поверхневого тиску.*

Introduction

Pituitary adenomas (PAs) are the most common primary benign intracranial tumors of the chiasmal and sellar region (CSR) which can cause compression of the optic nerve-chiasm complex (ONCC) [1, 2]. PAs have been reported to be the most common intracranial mass lesions [3–5].

The clinical picture depends on various characteristics including hormonal activity, direction of tumor extension, rate of growth, tumor size and mass effect on surrounding structures [6, 7].

The modified Hardy classification (1970) is that most commonly used to determine metric characteristics, with PAs grouped into four types based on their size: grade I (≤ 10 mm, within the sella microadenoma), grade II (10-20 mm, with a suprasellar extension within 10 mm of planum sphenoidale), grade III (20-40 mm, with a suprasellar extension ≤ 30 mm, distorting or invading the anterior third ventricle), and grade IV (≥ 40 mm, extending far beyond the sellar space, with lateral or multi-directional expansions (giant PA)) [8].

The absence of clinical manifestations of hormonal hypersecretion usually results in significant diagnostic delay and therefore non-functioning pituitary adenomas (NFPAs) may not be diagnosed until they cause mass effects to surrounding structures. Visual acuity (VA) and/or visual field impairment is a major clinical manifestation of an NFPA of a size not exceeding 40 mm. The tumor growth rate may vary for each patient, with PAs representing gradations of a spectrum from slowly growing tumors to rapidly growing aggressive neoplasms. Taken collectively, the above parameters of PA are of critical importance for selecting the treatment strategy and time frame [9, 10].

Mathematical modeling has been extensively used in ophthalmology to enable accurate diagnostic evaluation of patients, optimize treatment strategies, reduce the number of animal experiments and facilitate the development of novel technologies.

By constructing a simplified mathematical model, McIlwaine and colleagues (2005) [11] demonstrated that nasal fibers are subject to relatively greater pressures for any given external compressive force acting on the chiasm. Kosmorsky et al [12] used cadaveric specimens to measure the pressure in the temporal and central aspects of the chiasm simultaneously during compression of the chiasm from below with an expanding simulated tumor. They found that, during deformation the chiasm from below by a radially expanding mass analogous to a pituitary tumor, the central aspect of the chiasm consistently manifests a higher pressure than the temporal aspect. Wang and colleagues [13-15] reported on finite element modeling of optic chiasmal compression. Ex vivo experiment and finite modeling were utilized to investigate the biomechanics of human optic chiasm compression and explain the mechanism of bitemporal hemianopia arising as a result of chiasmal compression [16]. Compression of the chiasm induced high strains in the paracentral portions of the chiasm where the crossing optic nerve fibres are located. At an axonal level, the magnitude of strains affecting crossed fibres were greater than those affecting uncrossed fibres.

The concept of calculating the area of the zone of chiasmal pressure from a tumor and VA deficiency is a critically important aspect of ophthalmology and neurology. For this calculation, the size of the tumor

that exerts pressure on the surface of the optic chiasm and may result in vision deficiency is to be measured. Precise assessment of this area is important to determine relevant treatment strategies (like surgical intervention or radiotherapy) for decompressing the optic chiasm and preventing further vision loss. Using modern imaging techniques like magnetic resonance imaging (MRI) and computed tomography (CT) may be helpful for measuring tumor size and calculating the effect on visual function. This information is essential for developing individual treatment plans to preserve or restore visual function in patients with the tumors that affect the chiasm.

To the best of our knowledge, no study has reported on the assessment of surface pressure area.

The purpose of this study was to develop a mathematical model of chiasmal compression using a computer model of the area of surface pressure from the tumor.

Material and Methods

This study was conducted at the Department for Endonasal Cranial Base Endosurgery and Neuroophthalmology Unit, SI "Romodanov Neurosurgery Institute, National Academy of Medical Sciences of Ukraine", in 2018-2024. Mathematical modeling was done in cooperation with the Department of Software Engineering in Energy Industry, National Technical University of Ukraine "Igor Sikorsky Kyiv Polytechnic Institute".

The study was based on modeling and statistical analysis. This was a single-center, prospective cohort study. The study sample included 361 patients (54.7% were women and 45.3% were men; mean age, 54.3 ± 12.5 years; age range, 18–75 years) with PA and was normally distributed for tumor growth stage: group 1, early stage (small PAs, n = 115), group 2, moderately advanced stage (moderate-size PAs, n=157), group 3, advanced stage (giant PAs, n = 89). Patients were followed up for 24 months. Inclusion criteria were adults as defined by the WHO (18 years of older), presence of visual impairment (VA and/or visual field loss), surgical decompression of the ONCC as a result of subtotal or total tumor resection, and histological verification of the tumor. Exclusion criteria were tumors smaller than 10 mm in diameter, continued tumor growth, patients with signs of intracranial hypertension and ocular comorbidities, history of radiotherapy or radiosurgery, or medical decompression of the ONCC. Standardized examination techniques were used.

The sample was representative and large enough to provide for sufficient statistical power for analysis and making substantiated conclusions regarding the parameters examined. Patients underwent clinical neurological and ophthalmological examination before and after surgery. Additionally, they underwent comprehensive neuroimaging evaluation (MRI with contrast enhancement and CT scans of the brain) before surgery.

Optic coherence tomography (OCT) was conducted using a Revo NX instrument (Optopol Technology SA, Zawiercie, Poland). Optic disc excavation area, depth and volume, peripapillary retinal nerve fiber layer (RNFL) thickness, neuroretinal rim area, and macular ganglion cell complex (GCC) thickness were assessed by OCT.

Brain multislice computed tomography (MSCT) was conducted at the Neuroroentgenology Department of the institute using a Philips Brilliance 64 MSCT system (Philips Medical Systems, Best, the Netherlands) to obtain brain MSCT images in the three planes (slice thickness, 0.5 mm).

MRI was conducted at the Neuroradiology and Radiosurgery Department of the institute using a 1.5-T MRI system (Intera 1.5T/I system, Philips Medical Systems) to obtain conventional and contrast enhanced images in the three planes.

Neuroimaging techniques were utilized to determine the location (intrasellar, suprasellar, parasellar or infrasellar), extension (direction of tumor growth) and size of the tumor of the CSR, and the presence of hemorrhage, cyst formation, and lateralization, and relationship with surrounding structures.

The study followed ethical standards as outlined in the Declaration of Helsinki, and was approved by the Ethics Committee of SI "Romodanov Neurosurgery Institute, National Academy of Medical Sciences of Ukraine" (Minutes No. 5 dated December 13, 2019). All patients were informed about the specifics of the diagnostic and therapeutic procedures and provided written informed consent.

The modeling system is based on the comprehensive approach to representing anatomic structures using advanced computer graphics and modeling techniques. Utilizing Bézier curves and parametric modeling enables a high precision representation of anatomical structures and their deformations.

Bézier curves underpin the deformation modeling system, providing a smooth transition between control points, capability for accurate mathematical description of shape, effective shape control through control points, and preserve shape continuity in the presence of deformations. Using a tensor approach enables describing complex spatial deformations, allowing for nonlinear effects, preserving physical correctness of transformations, and controlling strains in a model.

A mathematical model is implemented through the following phases: model initiation (loading basic geometry, determining control points and setting initial parameters), calculation of deformations (computing displacement vectors, computing new vertex positions, and updating normals and texture coordinates), and optimization (smoothing resulting data curves, removing artifacts, and restructuring topology [if required]).

A powerful mathematical apparatus is a key element of the system and involves using splines to describe complex curved surfaces and deformation tensors to calculate changes in the shapes of objects. Surface interpolation is

performed between key points using optimized algorithms to enable smooth transitions and authentic reflections.

Technical implementation of the system provides for the use of dedicated biomedical modeling software with the integration of medical data imaging systems. An important aspect is the optimization of polygonal mesh and effective use of texture maps, which provides for a balance between model accuracy and computational efficiency.

Figs. 1 to 3 represent a series of 3D models that demonstrate different stages of deformation and transformation of objects. The visualization presented illustrates important aspects of deformation modeling.

Fig. 1 demonstrates normal texture of the neural tissue of the optic chiasm, whereas Fig. 2 demonstrates pathological changes induced by tumor compression of the chiasm with evidence of heterogeneous compressive deformation. Fig. 3 shows the final deformation result, demonstrating non-linear shape changes.

The evaluation of prerequisites for the use of least squares method included checking for multicollinearity between potential independent variables (the pressure zone area and RNFL thickness). There was a significant strong correlation ($r = –0.93$; $p < 0.001$) between the pressure zone area and RNFL thickness. This indicated a high risk of multicollinearity if these variables were included in the multiple regression model, which would lead to instability and incorrect interpretation of coefficients. It was decided to exclude the RNFL thickness from the

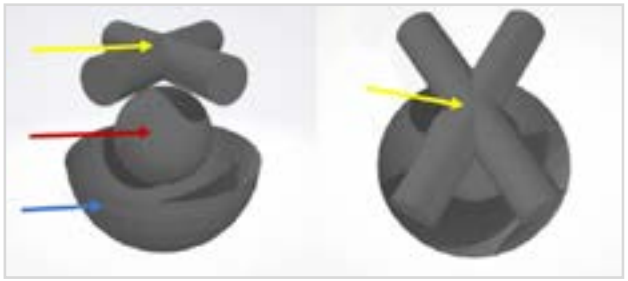

Fig. 1. 3D model of the chiasmal-sellar region: side view (A) and top view (B). The yellow arrow points to the optic chiasm, the red arrow to the pituitary adenoma, and the blue arrow to the sella turcica. Basic shape transformation is shown.

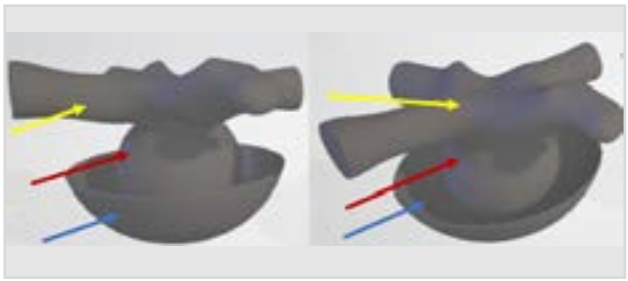

Fig. 2. 3D model of chiasmal compression by a pituitary adenoma: side view (A) and top view (B). The yellow arrow points to the optic chiasm, the red arrow to the pituitary adenoma, and the blue arrow to the sella turcica. Intermediate stage of transformation.

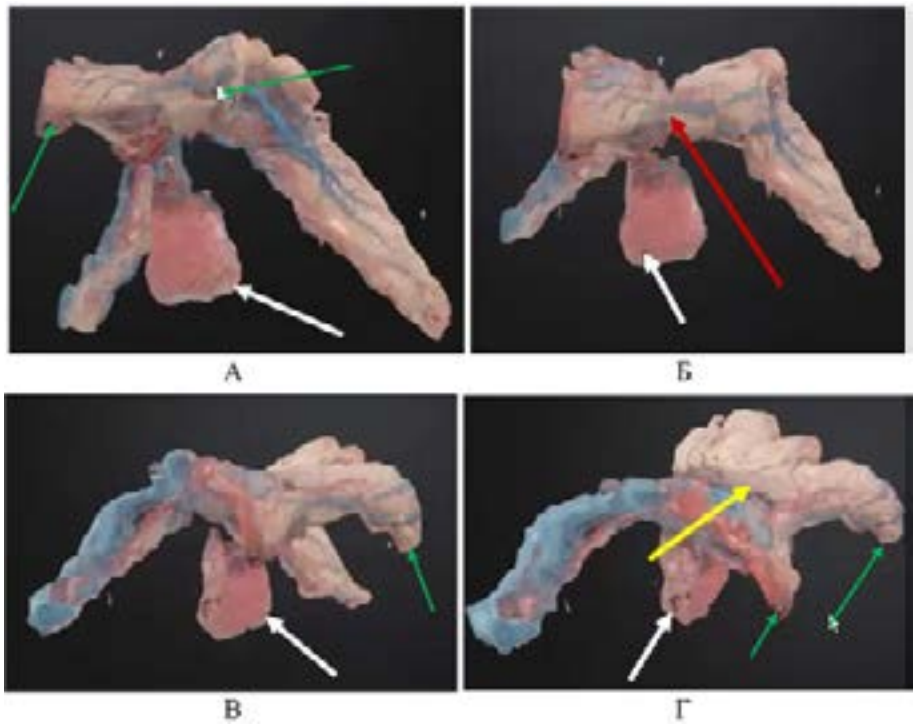

Fig. 3. 3D model of deformed optic nerve-chiasm complex: front view (A, B), side view (C), and top view (D).The yellow arrow points to the optic chiasm, the red arrow to the front surface of the optic chiasm, the green arrow to the intracranial portion of the optic nerves, and the white arrow to the pituitary adenoma. Intermediate stage of transformation. The final deformation result and complex spatial transformations are shown

final model to provide for stability and reliability of the regression equation. This decision was made because the pressure zone area was recognized as a primary mechanical factor (the cause) initiating the pathological process whereas the RNFL thickness was recognized as a structural consequence of compression. Therefore, regression analysis was focused on establishing a direct relationship between the area of pressure zone and VA. The final regression model was built as a univariate regression model, which allowed avoiding multicollinearity between independent variables.

SPSS Statistics v.30 and Microsoft Excel 2019 software were used for statistical analysis. The Kolmogorov-Smirnov test was used to check data distribution for normality. Quantitative variables are presented as mean and standard deviation (SD), and qualitative variables, as numbers and percentages. The Student t-test was used for two-group comparison of normally distributed data. The Mann-Whitney U test was used for two-group comparison of non-normally distributed data. Pearson correlation was used for normally distributed variables and Spearman's rank correlation was used for variables not normally distributed. Multiple regression analysis and logistic regression were used to develop predictive models. Statistical hypotheses were tested at the $p < 0.05$ level of significance. The level of significance $p < 0.05$ was assumed. The sample size was calculated a priori using G*Power 3.1.9.7 software to achieve a statistical power of 80% at an alpha level of 0.05 and assuming a large effect size (d = 0.5). Expert agreement was assessed using Kendall's coefficient of concordance (W). All calculations were performed taking in account current guidelines for performing statistical analysis of medical data and presenting study findings.

Results

At the first phase of the study, analysis of major clinical characteristics of the total sample (361 patients with PA) was performed. Patients were divided into three groups (stages) based on the size of the tumor: group 1, early stage (small PAs, n = 115), group 2, moderately advanced stage (moderate-size PAs, n=157), and group 3, advanced stage (giant PAs, n = 89). Because the mean defect (MD) had a rather large effect on the model, it was deemed reasonable to examine this effect separately, which will be performed in further studies.

Table 1 presents average values of the major parameters examined for the groups and statistical data for further research.

A comparative analysis among interpolating functions of linear, quadratic, cubic, power, hyperbolic and exponential regressions was conducted to determine the relationship y = y(x) between the growth stage and the area of the zone of pressure from a PA. Based on the comparison of approximation error and the closest values of the Fisher test, it was concluded that the relationship between the area of the zone of pressure from a tumor and tumor growth stage is best characterized by the exponential function У = 1.133 * 1.3612x. Because exponential regression demonstrated the largest determination coefficient (R2 = 0.9910) and the best agreement with clinical dynamics, it was selected as the basis for prediction (Table 2).

The calculation of the relationship between the area of pressure zone from a PA and VA is presented in Table 3. We compared approximation error and the closest values of the Fisher test, and concluded that the relationship between tumor pressure zone area and VA is best characterized by the exponential function z = 9.09 * 0.04y. Therefore, the relationship between tumor growth stage and VA can be established using the equation z(x) = 9.09*0.041.54x.

Given the above considerations, we performed a detailed analysis of the interrelationship of area of the zone of pressure from a PA, VA and RNFL thickness (Fig. 4).

Based on the analysis of the data obtained, the following patterns were found. There was a significant strong negative correlation ($r = –0.98$; $p < 0.001$) between pressure zone area and VA. That is, VA substantially decreases as pressure zone area increases. Additionally, there was a significant strong negative correlation ($r = –0.93$; $p < 0.001$) between

Table 1. Major parameters examined for the groups of patients (mean ± standard deviation and conventional units)

Characteristic	Group 1 (n=115)	Group 2 (n=157)	Group 3 (n=89)	P values
Average area of pressure zone from a PA (mm^2)	98.77 ± 11.86	200.74 ± 12.42	296.68 ± 11.24	p1-2<0.05 p1-3<0.05 p2-3<0.05
Area of pressure zone from a PA (CU)	100	200	300	-
Average RNFL thickness (μm)	92.4 ± 4.01	72.3 ± 4.04	52.2 ± 4.06	p1-2<0.05 p1-3<0.05 p2-3<0.05
RNFL thickness (CU)	100	90	40	-
Visual acuity	0.801 ± 0.06	0.603 ± 0.06	0.406 ± 0.06	p1-2<0.05 p1-3<0.05 p2-3<0.05

Notes: CU, conventional units; PA, pituitary adenoma; RNFL, retinal nerve fiber layer

Table 2. Exponential regression parameters describing the relationship between the growth stage of pituitary adenoma and tumor pressure zone area

	Resulting function	Correlation coefficient	Average approximation error	Critical value of Fisher's test	Actual value of Fisher's test
Exponential	$y=1.133*1.3612^x$	0.8788	2.1556%	10.128	10.172

Note: y, tumor growth stage; x, area of tumor pressure zone

Table 3. Correlations between the area of the zone of pressure from a pituitary adenoma and visual acuity

	Resulting function	Correlation coefficient	Average approximation error	Critical value of Fisher's test	Actual value of Fisher's test
Linear	$z=0.81y+0.81$	-	8.51%	3.18	10.39
Quadratic	$z=-0.97y^2+3.86y+4.8$	0.99	4.49%	5.79	552.17
Cubic	$z=2.07y^3+4.49y^2-5.55y+5.02$	0.9959	5.6%	6.59	321.58
Power	$z=0.7y-1.1$	0.62	50.86%	5.99	3.73
Hyperbolic	$z=0.6+0.65/y$	0.87	73.59%	5.99	19.49
Exponential	$z=9.09*0.04y$	0.86	3.28%	5.99	16.46

Note: z, area of tumor pressure zone; y, visual acuity

pressure zone area and RNFL thickness and a significant strong positive correlation ($r = 0.83$; $p < 0.001$) between the RNFL thickness and VA. Second-degree polynomial regression showed a perfect agreement with the data ($R^2 = 0.9910$). The plots demonstrated non-linear relationships between variables.

Both RNFL thickness and VA decreased with an increase in pressure zone area (with the groups showing separate ranges of Both RNFL thickness and VA); all the parameters worsened with an increase in tumor size, with the difference between groups being statistically significant ($p < 0.05$). VA was more influenced by pressure zone area than by RNFL thickness or MD. An increase in pressure zone area by 1 resulted in a decrease in VA by 0.109. An increase in pressure zone area resulted in a decrease in RNFL thickness, with an especially abrupt decline in RNFL thickness noted as pressure zone area exceeded 200 conventional units. An increase in RNFL thickness by 1 resulted in an improvement in VA by 0.0385. VA decreased non-linearly with increased pressure zone area, and the most abrupt decline in VA is noted when pressure zone area ranges between 100 and 200 conventional units. Both RNFL thickness and VA decreased with increased pressure zone area, which confirms the mechanism of damage to visual pathways.

The worst VA (0.42) and RNFL thickness (40 μm) values were noted for a pressure zone area of 300 conventional units, and the best VA (0.88) and RNFL thickness (100 μm) values, for the minimum pressure zone area (100 conventional units). Special attention should be given to cases in which pressure zone area exceeds 200 conventional units, resulting in abrupt worsening of the parameters.

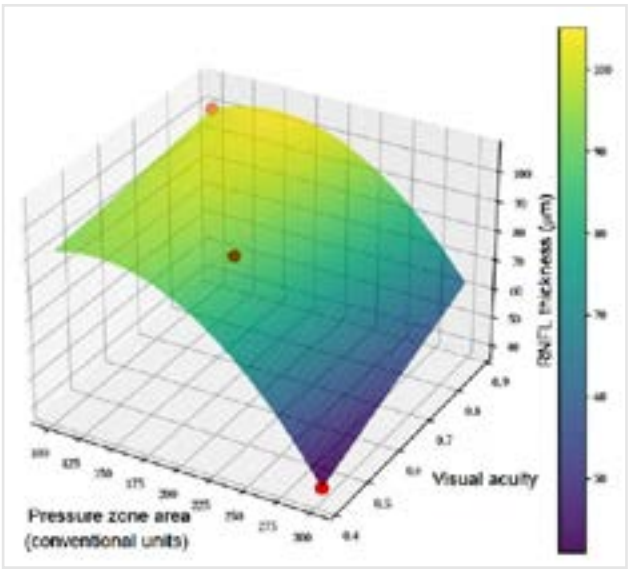

Fig. 4. 3D visualization of interrelationships between the area of the zone of chiasmal pressure, visual acuity and retinal nerve fiber layer (RNFL) thickness

Multivariate regression analysis based on the data obtained was conducted to find the equation z (x, y) of the relationship between the variables, where z is pressure zone area, x is VA, and y is RNFL thickness (Fig. 5).

Second-degree polynomial regression produced the following equation:

$z = 377.38 + 122.19x - 2.25y - 77.74x^2 - 2.91xy + 0.02y^2$,

where z is pressure zone area (conventional units), x is VA, and y is RNFL thickness (μm).

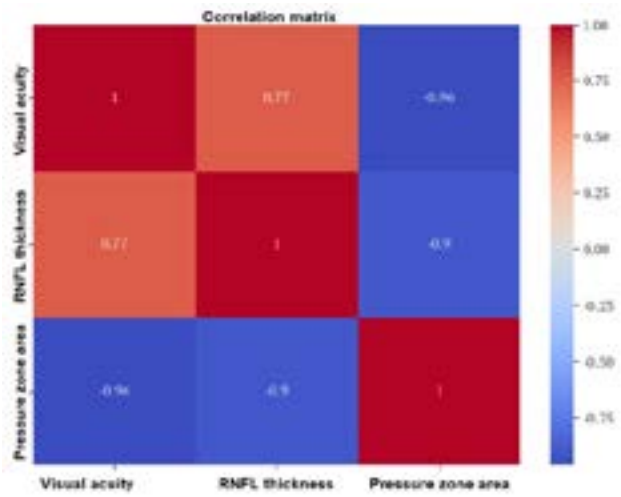

Fig. 5. Multivariate regression analysis

The mathematical model was developed using the entire data array of 361 patients. The high coefficient of determination value ($R^2 = 0.9910$ (99.10%)) indicates that the model is well fit.

The linear term (122.19x) and quadratic term ($–77.74x^2$) of VA has the largest effect, whereas the effect of the linear term of RNFL thickness (–2.25y) is smaller. Interaction between VA and RNFL thickness (–2.91xy) has some effect, and the effect of the quadratic term of RNFL thickness ($0.02y^2$) is the smallest. Pressure zone area strongly negatively correlated with VA and moderately negatively correlated with RNFL thickness, whereas VA positively correlated with RNFL thickness.

This equation can be used for predicting the area of pressure zone from a PA on the basis of VA and RNFL thickness.

Discussion

The study sample included 361 patients with PA (54.7% were women and 45.3% were men; mean age, 54.3 ± 12.5 years). Of these, 115 had early-stage PA, 157 had moderately advanced PA, and 89 had advanced PA. The difference between groups was not statistically significant.

The study has confirmed the efficacy of using both CT and MRI for assessing the size of the tumor. A mathematical model ($z = 377.38 + 122.19x – 2.25y – 77.74x^2 – 2.91xy + 0{,}02y^2$) was developed for predicting the area of pressure zone from a PA. Critical thresholds of the area of the zone of chiasmal pressure from a PA were determined. An especially abrupt decline in RNFL thickness was noted as pressure zone area exceeded 200 conventional units, and the worst VA (0.42) and RNFL thickness (40 μm) values were noted for a pressure zone area of 300 conventional units.

The model proposed has some substantial advantages compared to those developed previously by other researchers [11–13]. It is based on a complex approach that combines clinical data with mathematical modeling. This allows taking in account multiple parameters such as PZA (calculated with the help of 3D modeling), VA and RNFL thickness (determined with the help of OCT).

High model fitness ($R^2 = 0.9910$) and clear correlations between parameters provide for a reliable prediction of the area of pressure zone from a PA. This has an important practical value for detecting the pathology early and planning the treatment strategy early. Unlike studies reporting on the development of previous models [14–16], the current study used both modern imaging techniques and mathematical modeling. Critical thresholds of the area of pressure zone from a PA were determined and clear correlation relationships between the parameters were established, which allows for predicting the course of the disease. The model is easy to use in clinical practice and enables optimizing the treatment strategy.

Especially important was the establishment of a threshold value (200 conventional units) for pressure zone area, on exceeding which abrupt worsening of the parameters is noted. This allows early detection of patients at risk for disease progression to select the most appropriate time and strategy for treatment.

This study revealed clear relationships between tumor growth and changes in VA in patients. Average VA was 0.88 in patients with early PA, 0.56 in those with moderately advanced PA, and 0.42 in those with advanced PA. Especially important was the establishment of a non-linear nature of this relationship, with the most abrupt decline in VA noted when pressure zone area ranges between 100 and 200 conventional units.

We found a strong negative correlation ($r = –0.9754$) between pressure zone area and VA. Second-degree polynomial regression showed a high agreement with the data ($R^2 = 0.9910$), with an increase in the pressure zone area by 1 conventional unit resulting in a decrease in VA by 0.1091. A critical VA loss is observed when the pressure zone area exceeds 200 conventional units.

Additionally, we found a strong positive correlation ($r = 0.8312$) between RNFL thickness and VA. An increase in RNFL thickness by 1 resulted in an improvement in VA by 0.0385. The best VA (0.88) was found at an RNFL thickness of 100 μm, whereas a reduction in RNFL thickness to 40 μm was found to result in a critical decline in VA to 0.42.

The results obtained are confirmed by statistical significance and high R2 value. Further research is required to validate the model in an independent cohort of patients.

This study takes into account major ONCC compression parameters that can be mathematically calculated, and demonstrates their correlation with functional and morphometric parameters (VA and RNFL thickness, respectively). We are, however, aware that there are other factors (tumor density, tumor invasiveness, tumor growth rate, and vascular and individual anatomic parameters) that cannot be calculated using this model but have a significant effect on visual loss. Nevertheless, the integration of the model into routine MRI screening would create a new tool for the qualitative assessment of risk of

irreversible vision loss. The model enables personalizing the indication for surgery by clearly determining the time when the pressure zone area approaches a critical threshold of 200 conventional units, which is a signal for urgent intervention. A high accuracy of the model (R2 = 0.991) decreases the risk of unjustified delay of operation and guarantees that the prediction of vision loss is consistent with the actual degradation of visual pathways.

Therefore, the model developed represents an effective tool for the diagnosing and predicting the course of the disease, which is important for clinical practice.

Author Contributions

All authors reviewed the results and approved the final version of the manuscript.

Disclaimers

The views expressed in this article are solely those of the authors and do not necessarily represent the official position of their affiliated institution or any funding source.

Funding

No financial support was received for this study.

Conflict of Interest

The authors declare that they have no conflicts of interest related to this work.

Data Availability Statement

The datasets generated and/or analyzed during the current study are available from the corresponding author upon reasonable request. Due to institutional policy and patient confidentiality, raw data are not publicly available.

Abbreviations

CSR, chiasmal and sellar region; CT, computed tomography; MD, mean defect; MRI, magnetic resonance imaging; NFPA, non-functioning pituitary adenoma; OCT, optic coherence tomography; ONCC, optic nerve-chiasm complex; PA, pituitary adenoma; RNFL, retinal nerve fiber layer.

References

1. Wang EW, Gardner PA, Zanation AM. International consensus statement on endoscopic skull-base surgery: executive summary. Int Forum Allergy Rhinol. 2019;9(S3):S127-S144. doi:10.1002/alr.22327
2. Asa SL, Mete O, Perry A, Osamura RY. Overview of the 2022 WHO Classification of Pituitary Tumors. Endocr Pathol. 2022;33(1):6-26. doi:10.1007/s12022-022-09703-7
3. Rutkowski MJ, Chang KE, Cardinal T, et al. Development and clinical validation of a grading system for pituitary adenoma consistency. J Neurosurg. 2020;134(6):1800-1807. Published 2020 Jun 5. doi:10.3171/2020.4.JNS193288
4. Westall SJ, Aung ET, Kejem H, Daousi C, Thondam SK. Management of pituitary incidentalomas. Clin Med (Lond). 2023;23(2):129-134. doi:10.7861/clinmed.2023-0020
5. Mete O, Cintosun A, Pressman I, Asa SL. Epidemiology and biomarker profile of pituitary adenohypophysial tumors. Mod Pathol. 2018;31(6):900-909. doi:10.1038/s41379-018-0016-8
6. Fleseriu M, Biller BMK, Freda PU, et al. A Pituitary Society update to acromegaly management guidelines. Pituitary. 2021;24(1):1-13. doi:10.1007/s11102-020-01091-7.
7. Ntali G, Wass JA. Epidemiology, clinical presentation and diagnosis of non-functioning pituitary adenomas. Pituitary. 2018;21(2):111-118. doi:10.1007/s11102-018-0869-3.
8. Mooney MA, Hardesty DA, Sheehy JP, et al. Rater Reliability of the Hardy Classification for Pituitary Adenomas in the Magnetic Resonance Imaging Era. J Neurol Surg B Skull Base. 2017;78(5):413-418. doi:10.1055/s-0037-1603649
9. Mattogno PP, Zoli M, D'Alessandris QG, et al. Ultra-Early Treatment of Neurosurgical Emergencies with Endoscopic Endonasal Approach: Experience from Three Italian Referral Centers. J Clin Med. 2023;12(17):5471. Published 2023 Aug 23. doi:10.3390/jcm12175471.
10. Danesh-Meyer HV, Yoon JJ, Lawlor M, Savino PJ. Visual loss and recovery in chiasmal compression. Prog Retin Eye Res. 2019;73:100765. doi:10.1016/j.preteyeres.2019.06.001.
11. McIlwaine GG, Carrim ZI, Lueck CJ, Chrisp TM. A mechanical theory to account for bitemporal hemianopia from chiasmal compression. J Neuroophthalmol. 2005;25(1):40-43. doi:10.1097/00041327-200503000-00011.
12. Kosmorsky GS, Dupps WJ Jr, Drake RL. Nonuniform pressure generation in the optic chiasm may explain bitemporal hemianopsia. Ophthalmology. 2008;115(3):560-565. doi:10.1016/j.ophtha.2007.07.004.
13. Wang X, Neely AJ, McIlwaine GG, Lueck CJ. Multi-scale analysis of optic chiasmal compression by finite element modelling. J Biomech. 2014;47(10):2292-2299. doi:10.1016/j.jbiomech.2014.04.040.
14. Wang X, Neely AJ, McIlwaine GG, Tahtali M, Lillicrap TP, Lueck CJ. Finite element modeling of optic chiasmal compression. J Neuroophthalmol. 2014;34(4):324-330. doi:10.1097/WNO.0000000000000145
15. Wang X, Neely AJ, McIlwaine GG, Lueck CJ. Biomechanics of chiasmal compression: sensitivity of the mechanical behaviors of nerve fibers to variations in material property and geometry. Int J Comput Methods Eng Sci Mech 2016;17:165–71. doi.org/10.1080/15502287.2015.1084069.
16. Wang X, Neely AJ, Neeranjali S. Jain, Swaranjali V. Jain, Sanjiv Jain, Murat Tahtali, Gawn G. McIlwaine, Lueck CJ. Biomechanics of human optic chiasmal compression: ex vivo experiment and finite element modelling. Medicine in Novel Technology and Devices. 2022; 13:100113. doi.org/10.1016/j.medntd.2021.100113.